Catalysis Today 182 (2012) 16–24

Contents lists available at SciVerse ScienceDirect

Catalysis Today

journal homepage: www.elsevier.com/locate/cattod

The reactions of ethanol on TiO_2 and Au/TiO_2 anatase catalysts

A.M. Nadeem[b], G.I.N. Waterhouse[b], H. Idriss[a,*]

[a] Department of Chemistry, University of Aberdeen, Aberdeen, UK
[b] School of Chemical Sciences, University of Auckland, Auckland, New Zealand

ARTICLE INFO

Article history:
Received 10 June 2011
Received in revised form 13 August 2011
Accepted 16 August 2011
Available online 13 October 2011

Keywords:
TiO_2
Ethanol-TPD
Benzene formation
Ethanol dehydrogenation
Acetaldehyde condensation

ABSTRACT

The surface reactions of ethanol over TiO_2 and Au/TiO_2 nanoparticle catalysts were systematically investigated by temperature programmed desorption (TPD) and infra-red (IR) spectroscopic studies, in order to understand the effect of adding gold on the surface chemistry. Transmission Electron Microscopy (TEM) indicated that Au particles were mostly less than 10 nm in size; TiO_2 was of pure anatase form (XRD) of about 15–20 nm in size. Ethanol TPD on H_2-reduced TiO_2 showed that most reaction products desorbed in one single desorption domain at ca. 660 K. The main reaction product was ethylene (with a carbon selectivity of about 70%); other minor products were acetaldehyde, butene, and crotonaldehyde in decreasing order of yield. Ethanol TPD over H_2-reduced Au/TiO_2 was considerably different. First, a large fraction of the reaction products desorbed around 600 K; second the main desorption product was observed to be benzene. Infrared spectroscopy indicated that at room temperature both ethanol (1262 cm^{-1}, 1310 cm^{-1}, and 1398 cm^{-1}; due to O–H bending, CH_2 wagging, and CH_3 symmetric deformation modes, respectively) and ethoxide species (1047 cm^{-1}, 1073 cm^{-1}, 1093 cm^{-1}, and 1122 cm^{-1}; due to the stretching modes of CO and CC) are present with the former disappearing faster than the latter. In addition bands at 1634 and 1658 cm^{-1} attributed to ν(C–O), ν(C=C) and $\rho(CH_3)$ of adsorbed crotonaldehyde are seen when the ethanol dosed surface was flashed to 570 K. A scheme for the formation of the reaction products on TiO_2 and Au/TiO_2 is proposed in which benzene is formed on Au/TiO_2 by successive condensation reactions.

1. Introduction

The study of the reactions of alcohols on TiO_2 has many important technological applications. Ethanol, in particular, may be exploited as renewable energy carrier for generating hydrogen as well as a renewable feed for specialty chemicals. In addition, alcohols in general can act as simple model contaminants to test environmental cleaning strategies, one of which is photo-mineralization of organic contaminants to CO_2. Ethanol photo-reaction on M/TiO_2 (where M is a transition metal) for hydrogen production has been studied in some detail over the last decade [1–6] and it was found that Au/TiO_2 anatase has very high activity. The dark catalytic and non catalytic reactions of ethanol have been investigated previously over a wide range of model and real catalytic surfaces [7–17]. These studies indicated that ethanol adsorbs dissociatively to initially produce ethoxides and surface hydroxyls; the ethoxides are attached to surface metal cations while the hydrogen ions are attached to surface oxygen anions. These ethoxides generally undergo dehydrogenation and dehydration to give acetaldehyde and ethylene, respectively, depending on the nature of the oxide [7]. The factors effecting these two reactions include acid/basic site density [7,8], bond energy [7], electronegativity difference [7], Madelung potential of oxygen anions and metal cations [9], and the oxygen electronic polarisability of the oxides [10]. In general, large metal cation–oxygen anion bond energy (i.e. a large Madelung potential of oxygen anions), will favour dehydration over dehydrogenation. TiO_2 in that regard fits these requirements and has been shown to produce large amounts of ethylene as compared to acetaldehyde. Other products mostly resulting from acetaldehyde have also been observed for the reaction of ethanol over metal oxides. These include: crotonaldehyde (formed by β-aldolisation of acetaldehyde) [18], ethyl acetate (formed by dimerisation of two acetaldehyde molecules), acetates (formed by direct oxidation of acetaldehyde) [2], benzene (an intriguing reaction initially observed on Pt/CeO_2 and proposed to occur via a series of condensation steps (β-aldolisation) to give a C_6 unsaturated compounds that undergo dehydration followed by cyclisation steps to ultimately yield the thermodynamically stable compound, benzene) [19,20], furan [21] and butenes [7].

The deposition of gold nano-particles on TiO_2 for catalytic applications has been pursued for over a decade [22–43]. Since the pioneering work of Haruta which demonstrated the unique catalytic activity of Au/TiO_2 for the selective low-temperature CO oxidation [33], the number of reports describing the use of Au/TiO_2 as heterogeneous catalyst for thermal reactions has grown considerably. These works have elaborated how to prepare Au

* Corresponding author. Present address: SABIC T&I, Riyadh, Saudi Arabia.
E-mail addresses: h.idriss@abdn.ac.uk, idrissh@sabic.com (H. Idriss).

0920-5861/$ – see front matter © 2011 Elsevier B.V. All rights reserved.
doi:10.1016/j.cattod.2011.08.051

nanoparticles with a narrow size distribution strongly anchored on the surface of TiO_2 nanoparticles. Au/TiO_2 materials also have enormous promise as UV light driven photo-catalysts. Owing to the extensive research that has been conducted relating to Au nanoparticles supported on different metal oxides, a general consensus now exists on several aspects of the Au-oxide system. The size of the gold particles substantially affects the catalytic activity, and the gold clusters must be smaller than 5 nm for high catalytic activity to occur. However, in a very recent study it was observed that 5 nm limit is not needed for photo-catalytic hydrogen production from ethanol over Au/TiO_2 [6].

The aim of this work is to further understand the reactions of ethanol on titania supported Au nanoparticle catalysts. This paper explores the effect of added Au nanoparticles on the decomposition mechanisms of ethanol on TiO_2 in dark conditions in order to further probe into the specific chemical reaction pathways.

2. Experimental

2.1. Catalyst preparation

TiO_2 anatase nano-particles were prepared by the sol–gel hydrolysis of Ti(IV) isopropoxide and TiO_2-supported gold nanoparticle catalysts (Au loading = 8 wt.%) were prepared by the deposition–precipitation method with urea as follows. Anatase nanoparticles were prepared by the sol–gel hydrolysis of Ti(IV) isopropoxide. Briefly, Ti(IV) isopropoxide (284.4 g) was dissolved in isopropanol at 20 °C. Under vigorous stirring, milli Q water was then added slowly dropwise to the Ti(IV) isopropoxide solution resulting in the hydrolysis of the alkoxide and precipitation of hydrous titanium oxides. The final molar ratio of water:Ti(IV) isopropoxide in the reaction mixture was 55.5:1. The suspension was then left stirring for 24 h. The particles were subsequently collected by vacuum filtration, washed repeatedly with isopropanol, and then air dried for 2 days at 20 °C. Anatase nanoparticles were then obtained upon calcination of the dried powders at 400 °C for 2 h. The micron sized anatase powder used in this work was obtained from BDH chemicals. Titania-supported gold nanoparticle catalysts were prepared by the deposition–precipitation with urea (DPU) method. Under vigorous stirring, titania (2.5 g) was added to a 250 mL aqueous solution containing $HAuCl_4{\cdot}3H_2O$ (1.1 mM for Au loadings of 2%) and urea (0.42 M). The suspensions of TiO_2 particles were then heated to 85 °C, and kept at this temperature under continuous stirring for 8 h. The Au(III) impregnated titanias were collected by vacuum filtration, washed repeatedly with milli Q water, dried for 2 days at 20 °C in a dessicator over silica gel, and then calcined at 300 °C for 1 h to thermally reduce surface Au(III) cations to Au metal.

Detailed account of synthesis procedures for these materials can be found in a previous work [5]. The BET surface areas for all catalysts did not deviate from that of TiO_2 anatase alone ($107 \pm 5\ m^2\ g_{Catal}^{-1}$), while the cumulative pore volume $0.26\ cm^3\ g^{-1}$ and average pore radius 4.0 nm typical for the anatase TiO_2 support were also unchanged. XRD indicated that TiO_2 was pure anatase. XPS analyses were performed on a Kratos Axis Ultra spectrometer using mono-chromatized Al Kα X-rays ($h\nu$ = 1486.6 eV) and with the hemispherical electron energy analyzer operated in the hybrid lens mode. The take-off angle with respect to the specimen surface was 90°. The charge-compensating low-energy electron system was used to minimize specimen charging during X-ray irradiation. The binding energy scale was calibrated using adventitious hydrocarbon referencing (C 1s = 284.7 eV). TEM data for the characterization of the sample was collected at ANSTO (Sydney, Australia) using a JEOL 2010F TEM. Specimens were supported on carbon coated copper grids for analysis. Details of the analyses were reported in other studies [5,6] and will be outlined in brief below when needed to explain the results.

2.2. Infra-red spectroscopy

Infra-red spectra were obtained using a Nicolet (Nexus) Fourier transform spectrometer. Infrared spectra of adsorbed species were obtained at a resolution of $4\ cm^{-1}$ with 256 scans per spectrum. The adsorption of ethanol on sample catalysts was performed in a temperature programmable stainless steel IR cell. The sample catalysts were pressed into self-supporting discs (ca. 10 mm in diameter), and mounted into a gold-plated brass sample holder in the centre of the cell. The cell was equipped with removable CaF_2 windows (32 mm diameter, 4 mm thick) sealed with Viton O-rings. A type K thermocouple, welded into the centre of the cell in close proximity to the catalyst disc, was used to monitor the temperature. The cell was then connected to a vacuum line, and maintained at a base pressure (ca. 10^{-6} Torr) with a diffusion pump backed by a roughing pump. To remove surface contaminants, the TiO_2 and Au/TiO_2 catalysts were annealed under 20 Torr of oxygen at 673 K overnight, followed by evacuation under vacuum for 1 h while cooling to 300 K. Ethanol was injected via a vacuum line connected to the IR cell. After exposure the cell was pumped down to $<10^{-5}$ Torr. The surface temperature was then raised in specific increments. When the desired temperature was reached, the cell was then cooled to 300 K before collection of a spectrum. Spectra presented in this work are obtained by subtracting the spectrum of the catalyst sample prior to adsorption, from that of the sample after ethanol adsorption.

2.3. Temperature programmed desorption (TPD)

A detailed account of experimental procedures and the equipment used in the TPD studies can be found in previous works [5]. In brief it is as follows: 50 mg of catalyst was placed in a quartz U-shaped fixed bed reactor connected to a vacuum system with a typical base pressure of 1×10^{-7} Torr maintained by a diffusion pump with a liquid N_2 trap. The whole system was connected to a Spectra Vision quadrupole mass spectrometer to monitor the masses of interest. The mass spectrometer had a mass range from 1 to 200 amu, and could monitor 12 masses at one time when run in profile mode. Linear temperature ramping at a rate of $20\ K\ min^{-1}$ was achieved by using an accurate temperature ramping unit which consisted of a Kaif digital temperature controller integrated with a glass lined furnace and a K type thermocouple. Prior to TPD, the catalysts were reduced under H_2 at 673 K for 4 h or more. A range of different dosages of ethanol (ranging from 50 μL to 0.2 μL) was studied. It was found that 2–5 μL of ethanol are sufficient for surface saturation. The TPD presented in this work is conducted at saturation coverage. Ethanol was allowed to adsorb and equilibrate with the catalyst surface for 15 min. The reactor was pumped down to remove weakly adsorbed ethanol on the catalyst surface, as well as on the walls of the reactor, for 30 min. In addition, the ethanol mass fragment m/z = 31 $(CH_2OH)^+$ was monitored until the base line is again reached. Different mass fragments were recorded as function of temperature to monitor the desorption of products i.e. ethanol (m/z = 31, 29, 45, and 27), acetaldehyde (m/z = 29, 44, 15, and 43), ethylene (m/z = 28 and 27), methane (m/z = 16 and 15) water (m/z = 18 and 17), H_2 (m/z = 2), CO (m/z = 28 and 16), CO_2 (m/z = 44) as a function of temperature. Relative yields of all desorption products were determined following references [44] for the mass spectrometer sensitivity factor and [13,18,19] for the calculation method.

UV–Vis Spectra were performed using a Shimadzu double-beam UV-2100 spectrophotometer. The UV spectrophotometer

was equipped with an integrating sphere, having a 60-mm internal diameter. Spectra were measured in the range of 240–500 nm at a slit width of 2 nm. Au/TiO_2 and TiO_2 (anatase) samples were imprinted onto anhydrous barium sulfate powder, which was used as a support for UV reflectance spectroscopy. $BaSO_4$ is an inert, non-absorbing solid standard, which is an essential component of reflectance accessory. The baseline was done using $BaSO_4$ as the reference.

3. Results and discussion

The Au/TiO_2 catalyst was characterized by TEM, XRD, XPS, BET and diffuse reflectance UV–Vis measurements. XPS of the Au 4f region for Au/TiO_2 catalyst did not show deviation with respect to metallic Au [6] in agreement with a recent work using environmental XPS [45]. The BET surface area and pore sizes are given in Section 2 while XRD revealed the anatase phase of TiO_2 as well as broad features typical for nanocrystalline Au. Diffuse reflectance UV–Vis indicated the surface plasmon resonance of Au at ca. 560 nm similar to those observed recently by other workers for Au/TiO_2 materials [46]. TEM of Au/TiO_2 catalyst is presented and discussed below.

3.1. Adsorption and reactions of ethanol on Au/TiO_2

3.1.1. Temperature programmed desorption studies

Ethanol TPD was performed on both the TiO_2 and Au/TiO_2 catalysts. Preliminary results indicated that prior treatment under hydrogen or oxygen at atmospheric pressure slightly affected the distribution and desorption temperature of the reaction products. The effect was more pronounced with increasing Au loading. Reaction products always desorbed at lower temperatures in the case of oxygen treated (oxidized) catalysts as compared to hydrogen reduced catalysts. In this study, we are interested in examining the effect of added metallic Au on the surface reactions of ethanol on TiO_2. As a result, only results of the H_2-reduced catalysts are presented and discussed in this work while those of the O_2-treated catalysts will be provided in a separate study because of their relevance to other photo-catalytic processes.

3.1.2. Ethanol reactions on TiO_{2-x}

TPD products profile following ethanol adsorption at 300 K on H_2-treated TiO_2 (reduction ocuured at 673 K over night under about 10 mL/min H_2 1 atm.) is shown in Fig. 1. Based on the catalyst surface area (107 m^2/g_{Catal}) and number density of 5-fold coordinated Ti atoms on a TiO_2 surface (2 Ti atoms per 38.76 $Å^2$ = 5.16×10^{18} Ti atoms per 1 m^2), the number of Ti atoms available on the surface in 50 mg of TiO_2 loaded in the TPD reactor is equal to ca. 3×10^{19}. Since the amount of ethanol used was 1 μL (1.03×10^{19} molecules) and assuming that all the ethanol molecules in 1 μL of ethanol dosed are adsorbed, the coverage is ca. 0.4.

The reactivity of aliphatic alcohols with TiO_2 powders has been studied by using a number of different techniques and pretreatments, including temperature programmed desorption [5,47,48], and references therein]. In general, adsorption is largely dissociative yielding alkoxides and surface hydroxyl groups. In this work ethanol is seen to desorb in the temperature domain 380–700 K and accounted for 3.8% of the total product desorbed. The desorption profile can be de-convoluted to two peaks a small one at about 460 K followed by a large desorption at about 620 K. The large peak might be attributed to ethoxide and hydroxyl recombination on surface oxygen defects. The most pronounced desorption signal is that of ethylene at 665 K contributing 71.7% of the total product desorbed. Assuming that surface coverage was initially about 0.4, then the number of sites involved in ethoxide conversion to ethylene is about 0.3. Ethylene is formed by ethoxide dehydration which can be linked to ethoxides adsorbed on oxygen defected sites. Because

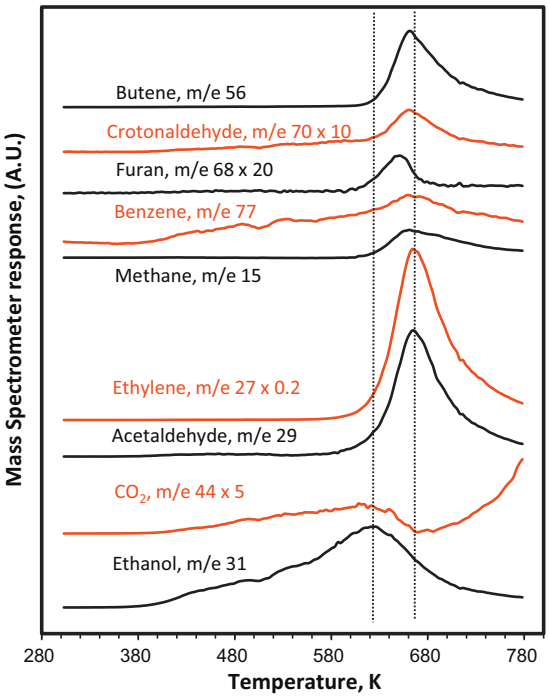

Fig. 1. TPD profile of different desorption products after ethanol adsorption at room temperature on H_2-reduced anatase TiO_2 nanoparticles.

the number of oxygen defects sites prior to adsorption cannot reasonably exceed 30% the dehydration reaction can be due in part to additional defects created during TPD. These defects can be created due to the removal of surface water as follows:

$$CH_3CH_2OH(g) + Ti_s\text{–}O_s \rightarrow CH_3CH_2OTi_s + OH(a) \quad (1)$$

$$2OH(a) \rightarrow H_2O(g) + V_O \quad (2)$$

(a) for adsorbed; V_O for surface oxygen vacancy; s for surface.

It is clear from the above equations that the number of V_O is at maximum ½ of the number of ethoxides/ethanol(a) and therefore can be at maximum equal to a surface coverage of 0.2. Therefore the formation of ethylene can be liked to a combination of surface oxygen defects created prior to adsorption and those formed during TPD among other factors.

A smaller fraction of ethoxides gave acetaldehyde by dehydrogenation (4%). It has been seen numerous times that the dehydrogenation reaction is far weaker on TiO_2 compared to the dehydration reaction. One can view this reaction as due to the removal of a hydride from the ethoxide as follows:

$$CH_3CH_2O(a) + OH(a) \rightarrow CH_3CHO(g) + H_2(g) + O_s \quad (3)$$

(a) for adsorbed; s for surface; (g) gas phase.

It is important to emphasize that the hydrogen removed from the ethoxide is a hydride ($H^{\delta-}$, i.e. a negatively charged H) that recombines with the hydrogen ion ($H^{\delta+}$) of the hydroxide to form H_2. The amount of acetaldehyde desorbing is not a true indicator of the extent of the dehydrogenation reaction on a reduced TiO_2 surface. There are other reactions which compete with acetaldehyde desorption. The most important of which has been observed previously on a reduced TiO_2 single crystal: the reductive coupling of carbonyl compounds to olefins known as McMurry reaction. Fig. 1 and Table 1 indicate considerable desorption of butene (9.6%) that is formed via the following reaction:

$$2CH_3CHO + 2V_O \rightarrow CH_3CH{=}CHCH_3 + 2O_s$$

Table 1
Carbon% yield and selectivity from ethanol-TPD on TiO_2 nanoparticles, after overnight reduction at 723 K with H_2.

Product	Peak temperature (K)	Carbon yield (%)	Carbon selectivity (%)
Ethanol	(380–550, 615)	0.2, 3.6	–
Acetaldehyde	660	4.0	4.2
Ethylene	660	71.7	74.5
Butene	660	9.6	10.0
Methane	660	1.8	1.9
Crotonaldehyde	385–605, 665	0.02, 0.4	0.02, 0.42
CO_2	610	0.1	0.1
Benzene	365–580, 650	0.6, 7.9	0.6, 8.2
Furan	385–580, 650	0.02, 0.1	0.02, 0.1
Total	LT, HT	0.84, 95.5	0.64, 99.3

LT and HT indicate total carbon% yield at low temperature and high temperature domains, respectively.
The carbon yield involves the corrected peak area of a desorbing product times its number of carbon. The carbon selectivity is the same taking away the reactant (ethanol in this case).

Together with butene desorption there is also a small desorption of crotonaldehyde (0.4%) via β-aldolisation (condensation of two acetaldehyde molecules followed by dehydration). Therefore the true activity of TiO_2 to acetaldehyde is close to 20% (taking into account reaction stoichiometry of the formation of butene and crotonaldehyde). In other words, the ratio dehydration to dehydrogenation is around 3. Intriguing is a non negligible amount of benzene formation. Benzene production was previously seen from ethanol during TPD on other surfaces [13,19,20] but has not yet been reported on H_2-reduced TiO_2. This reaction will be discussed in more detail below in the case of Au/TiO_2 catalyst as the addition of Au increases benzene formation considerably.

A small amount of methane with overall carbon selectivity of 1.9% desorbed at high temperature. CO_2 was seen to desorb in trace quantities at 610 K. This latter might have come from the high temperature decomposition of surface carbonates seen in IR studies (discussed below).

These results indicate that like previous studies on both single-crystal rutile TiO_2 (1 1 0) and (0 0 1) [11,49] and TiO_2 polycrystalline surfaces [5,47,48], alcohols decompose on reduced TiO_2 nanoparticle surfaces to produce surface-bound ethoxides, which are removed via two reaction channels during temperature programmed desorption experiments.

3.1.3. *Ethanol reactions on Au/TiO_{2-x}*

Fig. 2 shows TEM images of the 8 wt.% Au/TiO_2 catalyst. Most gold particles are of similar sizes, less than ca. 10 nm. As seen previously, the deposition with urea preparation method produces small gold particles in good contact with the TiO_2 anatase support, even at high Au loadings [6]. The TPD product profile following ethanol adsorption at 300 K on H_2-treated Au/TiO_2 is shown in Fig. 3.

In a previous study, the effect of Au loading on ethanol TPD reaction products was conducted for a series of H_2-treated Au/TiO_2 (Anatase) nanoparticle catalysts with 1, 2, 4 and 8 wt.% Au loading [50]. In general, Au loading affected the TPD desorption products temperature and distribution gradually. However the effect of added Au was most pronounced on the 8 wt.% Au catalyst as is presented here. We have previously studied this series of 0–8 wt.% Au/TiO_2 (Anatase) catalysts by TEM and XPS [6]. In general Au particle sizes increase with increasing Au loading from 1 to 8 wt.% while no change in the XPS Au 4f binding energies are seen when compared to that of bulk Au metal (binding energy of the XPS Au 4f at 84.0 eV).

Un-reacted ethanol (m/z 31) started to desorb at 380 K very similar to pure TiO_2 nano-particles, however, conversion to other products is seen about 60 K lower than in case of TiO_2 alone. The overall desorption of un-reacted ethanol is found to be 12% of the total carbon yield. Benzene was also desorbed at 380 K contributing 10.4% carbon yield at this temperature range and 50.3% at 585 K with other desorption products at higher temperature domain. Aside from benzene and ethanol, no other product was seen to desorb in the 380 K temperature domain.

The majority of the products desorbed at temperatures above 580 K in two desorption domains. In the case of pure TiO_2, only one desorption domain was observed. It can be noticed that Au loading shifts the product desorptions in the high temperature domain towards lower temperature. However there are still some desorption occurring due to TiO_2 sites not in proximity of Au. Therefore it appears that ethoxide species close to Au particles react differently than those on TiO_2 alone. The carbon selectivity for products desorbing at ~590 K was found equal to 76.6% while that at 640 K is equal to 11.7% for products desorbing. Carbon yields and carbon selectivities at the individual desorption temperatures are summarized in Table 2. It can be noticed that for the Au/TiO_2 catalyst, benzene is the most dominant desorption product with a total carbon selectivity of 69.1%, most of which desorbed at 590 K along with ethylene (dehydration), acetaldehyde (dehydrogenation), and other minor products including butene, crotonaldehyde and furan. Very small amount of methane with carbon selectivity of 0.5% was also detected. CO_2 was detected only at the highest temperature of 650 K.

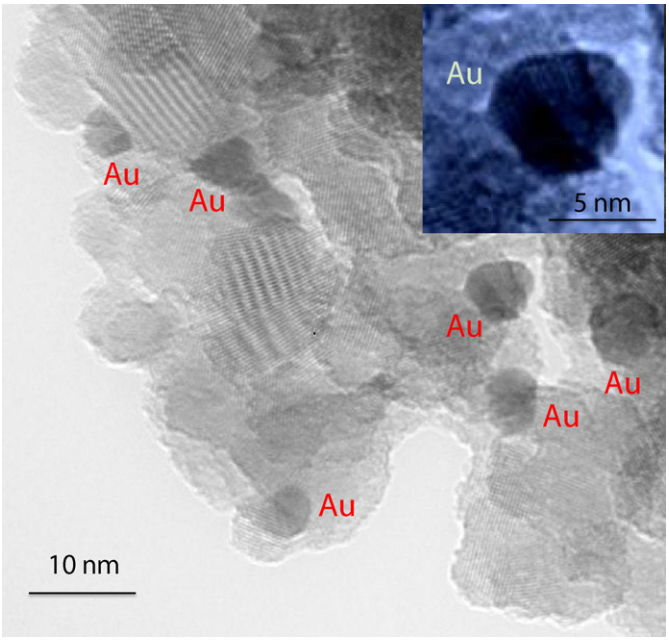

Fig. 2. TEM image of 8 wt.% Au/TiO_2 anatase. The square in the main picture is magnified and presented at the top right corner to highlight Au particles on top of the TiO_2 support.

Table 2
Carbon% yield and selectivity from ethanol-TPD on Au/TiO_2 nanoparticles, after overnight reduction at 723 K with H_2.

Product	Peak temperature (K)	Carbon yield (%)	Carbon selectivity (%)	Ratio MT/HT
Ethanol	355–500, 540	3.9, 8.3		
Acetaldehyde	585, 640	3.9, 1.6	4.4, 1.8	2.4/1
Ethylene	590, 640	7.0, 4.2	8.0, 4.8	1.7/1
Butene	600, 640	2.0, 1.7	2.3, 2.0	1.2/1
Methane	590, 640	0.5, 0.5	0.5, 0.5	1/1
Crotonaldehyde	600, 640	1.3, 1.8	1.5, 2.0	0.7/1
CO_2	650	0.5	0.6	
Benzene	355–477, 585	10.4, 50.3	11.8, 57.3	50/0
Furan	585	2.3	2.6,	2.3/0
Total	LT, MT, HT	14.3, 76, 9.8	11.8, 76.6, 11.7	6.5/1

LT, MT and HT indicate total % carbon yield at low, middle and the high temperatures, respectively.

3.2. Benzene formation on Au/TiO_{2-x}

On anatase TiO_2 ethylene was the major product desorbed with overall carbon selectivity of 74% while on Au/TiO_2 benzene was the major product with ~70% carbon selectivity. A simple explanation for the latter might be that ethylene is converted to benzene by a trimerization/dehydrgenation-type reaction. This explanation is most likely not accurate as discussed below.

Previous work by our group has shown the formation of crotonaldehyde from acetaldehyde over powder CeO_2 [51], reduced single crystal UO_2 (1 1 1) [52], powder UO_2 [21], U_3O_8 [21], Al_2O_3 [21]. Crotonaldehyde formation has also been observed, from acetaldehyde, over TiO_2 single crystals as well as powders [18]. Its formation requires both coordinatively unsaturated Ti cations to act as Lewis acid sites to bind acetaldehyde and a nearby basic site (oxygen anion) to abstract an α-H from acetaldehyde. The abstraction of a proton from the α position of acetaldehyde by lattice oxygen results in the formation of a $-CH_2CHO$(a) and a surface hydroxyl group. The former is a nucleophilic species which can react with the electrophilic carbonyl group of second acetaldehyde molecule adsorbed on an adjacent Ti cation to give an adsorbed aldol. The aldol thus formed further dehydrates to crotonaldehyde. However, the amount of crotonaldehyde desorbed during TPD is small over the Au/TiO_2 catalyst. This can be explained as follows. Once crotonaldehyde is formed, it can react with another adsorbed acetaldehyde (via the same β-aldolisation reaction) giving 2,4-hexadienal (see Eq. (4)). On contact with Au it may undergo C–H bond scission of the methyl group which after intramolecular cyclisation followed by H_2O elimination may give benzene as shown in Scheme 1.

$$CH_3CH{=}CHCHO + CH_3CHO \rightarrow CH_3CH{=}CHCH{=}CHCHO + H_2O \quad (4)$$

To summarize this section it is clear that Au particles had two noticeable effects. One decreasing the overall desorption at high temperature by up to 60 °C for the 8% Au/TiO_2 and two shifting the reaction selectivity from ethylene (dehydration) to acetaldehyde (dehydrogenation); the latter further react by condensation to benzene. This means that the abstraction of the H atom in the alpha position from the C–O (as a hydride) is favoured in the presence of Au compared to that of the H atom in the beta position of the C–O (as a proton) in the absence of Au.

The TiO_2 nanoparticles used in this work, have a high surface area (more adsorption sites) and small pore size (4 nm in size). This provides not only more active sites for re-adsorption but also hinders the diffusion of bulky molecules like 2,4-hexadienal. Reztova et al. [53] investigated the photoreactions of ethanol and acetaldehyde on TiO_2/carbon molecular sieve fibers (CMSF). They proposed that small titania particles may have a stronger binding energy than larger particles and which may stabilize acetaldehyde adsorption and facilitate further decomposition. The stronger binding energies of adsorbates on smaller particles compared to larger ones has been reported for metals; for example, the binding energies of H, OH, and CO increases with decreasing particle size for Pt [54].

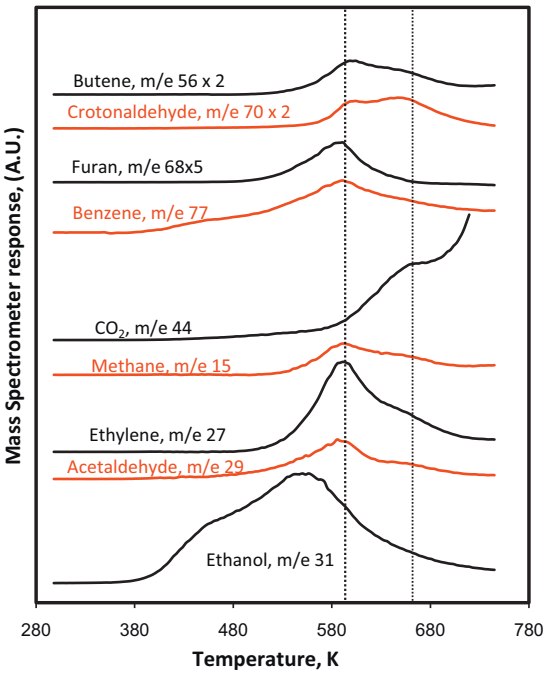

Fig. 3. TPD profile of different products after ethanol adsorption at room temperature on H_2-reduced Au/TiO_2.

3.3. IR results

Fig. 4 shows the IR spectra of ethanol adsorbed on H_2 reduced Au/TiO_{2-x}, collected after ethanol adsorption at 300 K followed by evacuation at the indicated temperatures. At 300 K, IR absorption bands characteristic for ethanol are seen and can be divided into three groups: bands in 1000–1200 cm^{-1} range corresponding to C–O and C–C stretching vibrations, bands in 1250–1500 cm^{-1} range correspond to CH_2, CH_3 and O–H bending vibrations and bands in 2800–3100 cm^{-1} range correspond to CH_2, CH_3 stretching vibrations.

The partial decrease in intensity of the CH_2, CH_3 stretching vibrations bands with increasing temperature is due to the removal of adsorbed ethanol from the surface. No change in position of these bands was noticed with heating but some qualitative change was evident in the absorption bands in the 980–1700 cm^{-1} range. Fig. 5 shows is magnified view of the 1690–990 cm^{-1} region of Fig. 4.

The absorption bands found in the room temperature spectra of this study, and a few previous studies and the corresponding vibrational modes of ethoxide, are given and compared in Table 3.

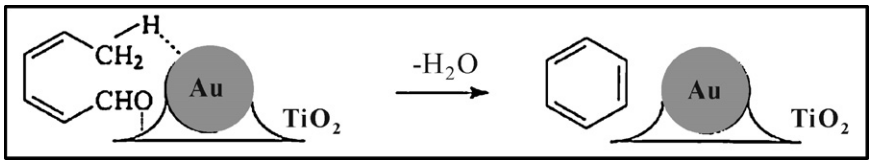

Scheme 1. Schematic of proposed mechanism for benzene formation over Au/TiO_2; 2,4-hexadienal is formed as shown in Eq. (4).

Table 3
IR vibrational frequencies and assignments for ethoxide species formed upon the adsorption of ethanol on Au/TiO_2 and on other catalysts.

Vibrational modes	This work	TiO_2 [5]	CeO_2 [59]	Au/CeO_2 [57]	Pd/CeO_2 [59]	Pt/CeO_2 [19]	Rh/CeO_2 [20]
Range, 100–1200 cm^{-1} (C–O and C–C stretching)							
νO–C (bidentate)	1047	1050	1057	1038	1037	1037	1038
νO–C (monodentate)	1122, 1146	1100	1107	1109	1078	1081	1080
νC–C	1071, 1093	−1070	–	1065	–	–	–
Range, 1250–1500 cm^{-1} (CH_2, CH_3 and O–H bending)							
$\omega(CH_2)$	1356	1356		1333	–	–	–
$\delta_s(CH_2)$	–	–	–	1362	–	–	–
$\delta_{as}(CH_2)$	1474	1473	1473	1478	1478	1480	1478
$\delta_s(CH_3)$	1378	1379	1383	1399	1397	1399	1399
$\delta_{as}(CH_3)$	1442	1447	–	1449	1451	1451	1450
$\delta_s(OH)$	1262	–	–	–	–	–	–
$\delta_s(H_2O)$	1638	–	–	–	–	–	–
Range 2800–3100 cm^{-1} (CH_2, CH_3 stretching)							
$\nu_s(CH_2)$	2870	2875	–	2875	2880	2878	2878
$\nu_{as}(CH_2)$	2932	2930	–	2933	2934	2933	2934
$\nu_s(CH_3)$	–	–	2836	2904	2909	2912	2911
$\nu_{as}(CH_3)$	2972	2975	2960	2971	2982	2977	2981

We focus our discussion primarily on the C–O stretching mode, as this vibrational mode is directly affected by the mode of adsorption. The absorption bands in the 298 K spectrum of this study are very similar to those observed in the previous IR measurement for TiO_2 following ethanol adsorption [55,56] indicating that Au deposition has either no or very small effect on ethanol adsorption at this temperature. This is in contrast to Au/CeO_2 system [57] where the ν(C–O) mode of ethanol is shifted to lower wavenumbers on adsorption on Au/CeO_2 compared to that observed on CeO_2 alone [58,59].

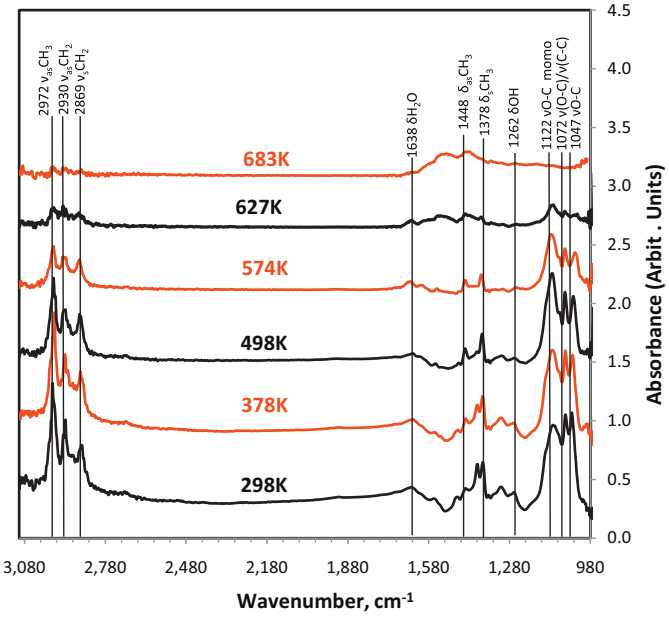

Fig. 4. FTIR spectra after adsorption of ethanol at RT on H_2-reduced Au/TiO_2 and subsequent heating at the indicated temperature. All spectra were recorded at room temperature.

3.4. Molecular ethanol desorption

In the spectrum collected at room temperature, the bands at 1262 cm^{-1}, 1310 cm^{-1}, and 1398 cm^{-1} are due to O–H bending, CH_2 wagging, and CH_3 symmetric deformation of $C_2H_5OH_{(a)}$, respectively The intensity of these bands started to decrease with increasing temperature and disappeared by 575 K indicating that molecular ethanol has been removed and/or converted into other surface species; the OH bending mode was still present (albeit attenuated) but it is most likely due to surface hydroxyls and not to the OH mode of ethanol.

Fig. 6 presents the decay of ethanol (1398 cm^{-1}) and ethoxide (1122 m^{-1}) IR signals together with ethanol desorption during TPD. No attempt was made to correct for the changes in intensity with surface concentration as the objective of the figure is to qualitatively correlate desorption and surface species evolution. This figure is explained in more detail below.

3.5. Ethoxide desorption/reactions

In the spectrum collected at room temperature, IR absorption bands at 1047 cm^{-1}, 1073 cm^{-1}, and 1121 cm^{-1} correspond to C–O and C–C stretching modes of ethoxide adsorbed on the catalyst surface. Further identification of adsorption modes of ethoxides can be made by comparing the C–C and C–O stretching frequencies with the previous work by Wu et al. [55]. At 298 K, the absorption bands for $C_2H_5O_{(a)}$ are at 1047 cm^{-1}, 1073 cm^{-1}, 1093 cm^{-1} and 1122 cm^{-1}. Among these bands, the bands at 1047 cm^{-1}, 1122 cm^{-1}, and 1146 cm^{-1} can be assigned to the C–O stretching and the bands at 1071 cm^{-1} and 1093 cm^{-1} to the C–C stretching of ethoxides. Among C–O stretching bands, 1047 cm^{-1} corresponds to bidentate while band at 1122 cm^{-1} corresponds to a monodentate ethoxide species. It is now worth comparing these results to TPD results obtained from the same surface where some useful conclusions could be made. The dotted line in Fig. 6 indicates the decrease in IR peak areas of the 1121 cm^{-1} band with temperature. It is clear that this form of ethoxide is affected very little until 500 K, but above this temperature it starts to convert into other

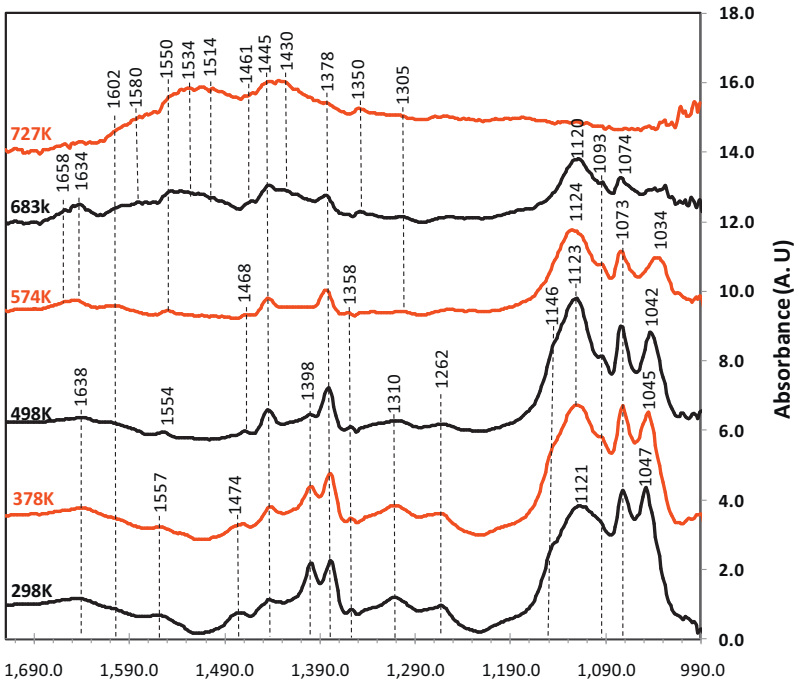

Fig. 5. FTIR spectra in the 1700–990 cm^{-1} range after ethanol adsorption on Au/TiO_2 and subsequent heating at the indicated temperature. All spectra were recorded at room temperature.

products. Molecular ethanol starts decreasing as soon as the temperature of the surface is increased above room temperature and is completely removed at temperatures between 500 K and 575 K. Interestingly it also appears that adsorbed ethanol molecules do not convert to ethoxide species with increasing temperature but instead desorb; since the intensity of ethoxide related vibrational modes does not increase but actually gradually decrease. This may indicate that ethanol molecules are adsorbed on sites that do not allow for O–H bond dissociation. These sites might be adjacent to Au clusters. It is also worth mentioning the continuous shift of the peak at 1047 cm^{-1}, corresponding to bidentate ethoxides on the surface, towards lower wavenumbers with increase in temperature. This might be due to decreasing of the population of surface adsorbates that result in slight stabilization (less dipole–dipole repulsion). The two bands for ethoxides at 1047 and 1121 cm^{-1} are both attenuated with increasing temperature, but do not show the same temperature dependence. Their ratio changes considerably with increasing temperature. The ratio 1047 cm^{-1} to 1121 cm^{-1} is 1.13 at 298 K then steadily decreases to become 0.6 at 575 K. The reason for this is unclear as one would expect that the monodentate species (1121 cm^{-1}) to disappear before the bi-dentate species (1047 cm^{-1}). One possible explanation is that the mono-dentate species at higher temperature are those of ethoxide species that have migrated to surface oxygen vacancies as has been observed by STM over TiO_2 (1 1 0) rutile single crystal surface [58].

3.6. Identification of possible oxidation/coupling products

During TPD it was found that ethoxides started to convert into other products at around 505 K. These reactions mainly include dehydration, dehydrogenation, condensation and coupling products. The presence of the condensation product crotonaldehyde can be confirmed by the appearance of two distinct IR bands at 1634 and 1658 cm^{-1} attributed to ν(C–O), ν(C=C) and $\rho(CH_3)$ of adsorbed crotonaldehyde [19,59]. Desorption of crotonaldehyde along with other coupling products were also noticed around this temperature during TPD. Higher temperatures caused ethoxide decomposition and removal from the surface indicated by the disappearance of all its characteristic peaks and appearance of completely new complex band structure in 1350–1650 cm^{-1} region. The peaks in this region can be assigned to carbonate species formed on the surface [60]. Carbonate species started to appear at 685 K and were the only species detected by IR at temperature 727 K. During TPD the other higher carbon containing products that desorbed were benzene, furan, and butene. The absence of IR bands attributed to any of these is expected as their desorption is reaction limited. Butene desorption occurs via pinacolate C–O bond dissociation. It is however not possible to distinguish between pinacolate and ethoxides by IR under the conditions of our experiments. Furan desorption from ethanol has also been seen on other systems from ethanol [61], acetaldehyde [21], ethylene [62] and acetylene [63] where the reaction

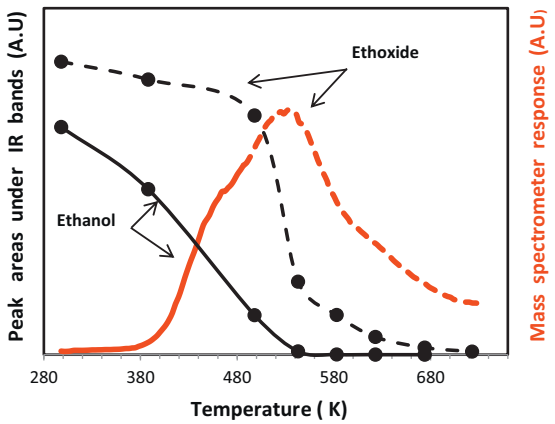

Fig. 6. Ethanol desorption from the Au/TiO_2 surface. Red line: ethanol desorption profile during TPD; solid thin line: decrease in 1398 cm^{-1} IR band area corresponding to molecular ethanol; dotted thin line: decrease of the IR band at 1121 cm^{-1} bands corresponding to mono-dentate ethoxide species. (For interpretation of the references to color in this figure legend, the reader is referred to the web version of the article.)

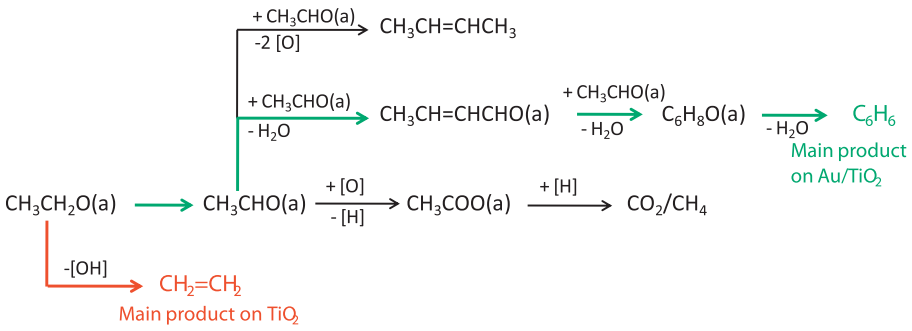

Scheme 2. Reaction mechanism for the formation of ethylene on TiO_2 and benzene on Au/TiO_2 starting from ethoxide species. Other minor reactions are neglected.

mechanism has been discussed in some detail; its minor contribution here does not allow us to track its formation by IR.

Owing to the presence of Au on TiO_2, the presence or absence of possible oxidation product of ethanol was carefully studied. Oxidation of ethanol may result in the formation of acetic acid, acetates, acetaldehyde and CO_2. Acetic acid is represented by a 1680 cm^{-1} band due to carbonyl stretching and acetate is represented by 1453 and 1535 cm^{-1} bands due to –COO– symmetric and antisymmetric stretching, respectively. No evidence for either of these species was found in this work. Also, the absence of spectral features for acetaldehyde at 1691 cm^{-1} ν(C=O), 1443 cm^{-1} $\delta_{as}(CH_3)$, 1377 cm^{-1} $\delta_s(CH_3)$, 1350 cm^{-1} indicated that the energy barrier for its formation from ethoxide species is higher than that of its adsorption.

Scheme 2 summarizes the main observed reaction products for ethanol decomposition over TiO_2 and Au/TiO_2, and gives likely mechanisms for product formation; products derived from ethoxides were mainly ethylene on TiO_2 and benzene over Au/TiO_2.

4. Conclusion

The surface reactions of ethanol on bare and Au nanoparticle modified anatase TiO_2 nanoparticle catalysts were successfully probed using a combination of TPD and FTIR spectroscopy. Ethanol decomposed on the bare TiO_2 support to yield surface ethoxide species, which decomposed via several reaction channels at 673 K to yield predominantly ethylene (ca. 71.7% carbon yield), and lesser amounts of butene (9.6%), acetaldehyde (4.0%), methane (1.8%). Small amounts of benzene, CO_2 crotonaldehyde and furan were also produced. Depositing Au nanoparticles on the surface of the anatase TiO_2 support dramatically changed the surface chemistry, surface energetics and relative distribution of these products. The main product of ethanol decomposition on Au/TiO_2 was benzene (ca. 60.7% carbon yield) which desorbed at 600 K, along with lesser amounts of the other reaction products seen for the bare TiO_2 catalyst. The high selectivity of the Au/TiO_2 catalyst for benzene formation is rationalised in terms a scheme whereby β-aldolisation reactions of acetaldehyde create a surface 2,4-hexadienal intermediate, which subsequently undergoes Au nanoparticle induced C–H bond scission of the methyl group of 2,4-hexadienal, then intramolecular cyclisation followed by H_2O elimination to give benzene. This work suggests that supported Au nanoparticle catalysts may useful for the synthesis of aromatic molecules from aliphatic alcohols.

Acknowledgements

The authors would like to thank AINSE Ltd for providing financial assistance through a Research Award (AINGRA09119) to enable TEM work on the Au/TiO_2 catalyst to be conducted. The support of Mark Blackford (ANSTO) in collecting the TEM data is also acknowledged. A.M. Nadeem thanks the HEC Pakistan for their finance through a PhD Scholarship.

References

[1] G.R. Bamwenda, S. Tsubota, T. Nakamura, M. Haruta, J. Photochem. Photobiol. A 89 (1995) 177.
[2] Y.Z. Yang, C.-H. Chang, H. Idriss, Appl. Catal. B: Environ. 67 (2006) 217.
[3] A.E. Raevskaya, A.V. Korzhak, A.L. Stroyuk, S.Y. Kuchmii, Theor. Exp. Chem. 45 (2009) 343.
[4] A.V. Korzhak, N.I. Ermokhina, A.L. Stroyuk, V.I. Litvin, V.K. Bukhtiyarov, P.A. Manorik, V.G. Il'in, Theor. Exp. Chem. 41 (2005) 26.
[5] M.A. Nadeem, M. Murdoch, G.I.N. Waterhouse, J.B. Metson, M.A. Keane, J. Llorca, H. Idriss, J. Photochem. Photobiol. A: Chem. 216 (2010) 250.
[6] M. Murdoch, G.W.N. Waterhouse, M.A. Nadeem, M.A. Keane, R.F. Howe, J. Llorca, H. Idriss, Nat. Chem. (2011), doi:10.1038/nchem.1048.
[7] H. Idriss, M.A. Barteau, Adv. Catal. 45 (2000) 261, and references therein.
[8] H. Idriss, E.G. Seebauer, J. Mol. Catal. A: Chem. 152 (2000) 201.
[9] S.V. Chong, T.R. Griffiths, H. Idriss, Surf. Sci. 444 (2000) 187.
[10] H. Idriss, E.G. Seebauer, Catal. Lett. 66 (2000) 139.
[11] A.M. Nadeem, J.M.R. Muir, J.B. Metson, H. Idriss, Phys. Chem. Chem. Phys. 13 (2011) 7637.
[12] C. Diagne, H. Idriss, A. Kiennemann, Catal. Commun. 3 (2002) 565.
[13] P.Y. Sheng, A. Yee, G.A. Bowmaker, H. Idriss, J. Catal. 208 (2002) 393.
[14] V. Fierro, V. Klouz, O. Akdim, C. Mirodatos, Catal. Today 75 (2002) 141.
[15] J.P. Breen, R. Burch, H.M. Coleman, Appl. Catal. B: Environ. 39 (2002) 65.
[16] S. Cavallaro, S. Freni, J. Hydrogen Energy 21 (1996) 465.
[17] G.I.N. Waterhouse, M. Murdoch, J. Llorca, H. Idriss, Int. J. Nanotechnol. 9 (2012) 113.
[18] H. Idriss, K.S. Kim, M.A. Barteau, J. Catal. 139 (1993) 119.
[19] A. Yee, S.J. Morrison, H. Idriss, J. Catal. 191 (2000) 30.
[20] A. Yee, S.J. Morrison, H. Idriss, Catal. Today 63 (2000) 327.
[21] H. Madhavaram, H. Idriss, J. Catal. 224 (2004) 358.
[22] Y. Wu, H. Liu, J. Zhang, F. Chen, J. Phys. Chem. C 113 (2009) 14689.
[23] B.K. Min, J.E. Heo, N.K. Youn, O.S. Joo, H. Lee, J.H. Kim, H.S. Kim, Catal. Commun. 10 (2009) 712.
[24] V. Rodriguez-Gonzalez, R. Zanella, G. del Angel, R. Gomez, J. Mol. Catal. A: Chem. 281 (2008) 93.
[25] V. Iliev, D. Tomova, L. Bilyarska, G. Tyuliev, J. Mol. Catal. A: Chem. 263 (2007) 32.
[26] R.S. Sonawane, M.K. Dongare, J. Mol. Catal. A: Chem. 243 (2006) 68.
[27] A. Orlov, M.S. Chan, D.A. Jefferson, D. Zhou, R.J. Lynch, R.M. Lambert, Environ. Technol. 27 (2006) 747.
[28] A. Dobosz, A. Sobczynski, Monatsh. Chem. 132 (2001) 1037.
[29] M. Haruta, Catal. Today 36 (1997) 153.
[30] S. Lee, C. Fan, T. Wu, S.L. Anderson, J. Am. Chem. Soc. 126 (2004) 5682.
[31] A.S.K. Hashmi, G.J. Hutchings, Angew. Chem. Int. Ed. 45 (2006) 7896.
[32] A. Corma, H. Garcia, Chem. Soc. Rev. 37 (2008) 2096.
[33] M. Haruta, J. Catal. 115 (1989) 301.
[34] G.R. Bamwenda, S. Tsubota, T. Nakamura, M. Haruta, Catal. Lett. 44 (1997) 83.
[35] M. Valden, X. Lai, D.W. Goodman, Science 281 (1998) 1647.
[36] M.S. Chen, D.W. Goodman, Acc. Chem. Res. 39 (2006) 739.
[37] F. Boccuzzi, A. Chiorino, J. Phys. Chem. B 104 (2000) 5414.
[38] B. Schumacher, V. Plzak, M. Kinne, R.J. Behm, Catal. Lett. 89 (2003) 109.
[39] M. Haruta, A. Ueda, S. Tsubota, R.M. Torres Sanchez, Catal. Today 29 (1996) 443.
[40] G.C. Bond, D.T. Thompson, Gold Bull. 33 (2000) 41.
[41] F. Cosandey, T.E. Madey, Surf. Rev. Lett. 8 (2001) 73.
[42] R. Meyer, C.S. Lemire, K.H. Shaikhutdinov, J. Freund, Gold Bull. 37 (2004) 72.
[43] K. Minato, T. Susaki, S. Shiraki, H.S. Kato, M. Kawai, K.-I. Aikaa, Surf. Sci. 566–568 (2004) 1012.
[44] E.I. Ko, J.B. Benziger, R.J. Madix, J. Catal. 62 (1980) 264.
[45] S. Porsgaard, P. Jiang, F. Borondics, S. Wendt, Z. Liu, H. Bluhm, F. Besenbacher, M. Salmeron, Angew. Chem. 123 (2011) 2314.
[46] Y. Borensztein, L. Delannoy, A. Djedidi, R.G. Barrera, C. Louis, J. Phys. Chem. C 114 (2010) 9008.

[47] V.S. Lusvardi, M.A. Barteau, W.E. Farneth, J. Catal. 153 (1995) 41.
[48] V.S. Lusvardi, M.A. Barteau, W.R. Dolinger, W.E. Farneth, J. Phys. Chem. 100 (1996) 18183.
[49] K.S. Kim, M.A. Barteau, J. Mol. Catal. 63 (1990) 103.
[50] M.A. Nadeem, G.I.N. Waterhouse, J.B. Metson, J. Llorca, H. Idriss; in preparation.
[51] H. Idriss, C. Diagne, J.P. Hindermann, A. Kiennemann, M.A. Barteau, J. Catal. 155 (1995) 219.
[52] S.V. Chong, H. Idriss, J. Vac. Sci. Technol. A 19 (2001) 1933.
[53] T. Reztova, C.-H. Chang, J. Koresh, H. Idriss, J. Catal. 185 (1999) 223.
[54] S. Mukerjee, J. McBreen, J. Electroanal. Chem. 448 (1998) 163.
[55] W.-C. Wu, C.-C. Chuang, J.-L. Lin, J. Phys. Chem. B 104 (2000) 8719.
[56] G.A.M. Hussein, N. Sheppard, M.I. Zaki, R.B. Fahim, J. Chem. Soc. Faraday Trans. 87 (1991) 2655.
[57] P.Y. Sheng, G.A. Bowmaker, H. Idriss, Appl. Catal. A: Gen. 261 (2004) 171.
[58] H. Idriss, Platinum Metals Review 48 (2004) 105.
[59] A. Yee, S.J. Morrison, H. Idriss, J. Catal. 186 (1999) 279.
[60] G. Busca, V. Lorenzelli, Mater. Chem. 7 (1982) 89.
[61] H. Madhavaram, H. Idriss, J. Catal. 184 (1999) 553.
[62] H. Madhavaram, H. Idriss, Stud. Surf. Sci. Catal. 110 (1997) 265.
[63] H. Madhavaram, H. Idriss, J. Catal. 206 (2002) 155.